JSEE Vol. 26, No. 2, 2024 DOI: 10.48303/jsee.2024.2006297.1068

Research Paper

Earthquake Nowcasting: Retrospective Testing in Sarpol-e Zahab, Iran

Majid Mahood

1. Assistant Professor, Seismological Research Center, International Institute of Earthquake Engineering and Seismology (IIEES), Tehran, Iran, m.mahood@iiees.ac.ir

Received: 05/07/2023
Revised: 27/02/2024
Accepted: 17/03/2024

ABSTRACT

Sarpol-e Zahab, in the west of Iran, is subjected to a high earthquake risk. Located in the north part of the Zagros seismic belt and is surrounded by several active faults that show some M7+ earthquake records. Nowcasting refers to the process of determining the uncertain state of the seismicity at the present time by indirect means for the seismically active regions, where the goal is to estimate the current state of risk, the current state of the fault system, and its current level of progress through the earthquake cycle. The local catalog of earthquakes is used, using "small" earthquakes to determine the level of hazard from "large" earthquakes in the region. To evaluate the statistical distribution of the inter-event counts of small events that occur between large events, the natural time concept was used rather than clock time (Origin Time of Earthquake). This method does not involve any model other than the idea of an earthquake cycle. Rather, a specific radius and a specific large earthquake magnitude of interest are defined, ensuring that we have enough data to span at least ~10 or larger earthquake cycles in the region. We then compute the earthquake potential score (EPS) which is defined as the cumulative probability distribution P (n<n(t)) for the current count n(t) for the small earthquakes in the region. The EPS was calculated as the total number of small earthquakes after the last large occurrence in the studied area. EPS is therefore the current level of hazard and assigns a number between 0% and 100% to every region so defined, thus providing a unique measure. Physically, the EPS corresponds to an estimate of the level of progress through the earthquake cycle in the defined region at the current time. We have determined the EPS values to consider events of Mw≥ 4.4 within two different radii (250 and 350 km) around Sarpol-e Zahab. The EPS values for Sarpol-e Zahab at 250 km corresponding to Mw?5.5 and six events were found to be almost 0.86 and 0.97, respectively, while at 350 km these values are equal to 0.73 and 0.50 for Mw≥ 5.5 and six events, respectively.

Keywords:
Sarpol-e Zahab, Nowcasting; Natural Time; Earthquake Potential Score (EPS); Zagros; Iran

1. Introduction

Studying the seismic hazard and evaluating and predicting the seismically active areas require knowledge of earthquake cycles and current state of fault system. The Alpide-Himalayan belt in Iran is defined by a broad band of diffused seismicity and contains several mobile belts surrounding small and relatively stable blocks. The Iranian Plateau, characterized by active faulting, active folding, recent volcanic activities, mountainous terrain, and variable crustal thickness, has been frequently struck by earthquakes resulting in the massive loss of life. The active tectonics of Iran is dominated by the northward motion of Arabia with respect to Eurasia. Berberian (1976) has divided Iran into four major seismotectonic zones, viz., Zagros active folded belt, central Iran, Alborz and Koppeh-Dagh in northeast Iran. Shortening and earthquake deformation within

Iran is mainly accommodated by distributed faulting in the Zagros, Alborz, Kopeh-Dagh and west of the Lut block in Kerman Province. Convergence between Eurasia and Arabia varies along the Zagros belt (Gentili et al., 2019; Walker et al., 2003). The persistent tectonic activity causes high seismicity throughout the region including a number of devastating earthquakes, such as the 1978 Tabas earthquake (M_w 7.3), 1987 Qaenat earthquake (M_w 7.2), 1990 Rudbar earthquake (M_w 7.4), 2003 Bam earthquake (M_w 6.6), 2012 Ahar-Varzaghan earthquakes (M_w 6.5 and 6.3), 2013 Saravan-Khash intraslab normal-faulting earthquake (M_w 7.7) in the Makran subduction zone, and the most recent 2017 Sarpol-e Zahab earthquake (M_w 7.3) in the Iran-Iraq border (Figure 1).

On 12 November 2017, at 21:48 local time (18:18 GMT), a destructive earthquake (M_w 7.3) occurred 5 km north of Ezgeleh and 43 km north of Sarpol-e Zahab (in Kermanshah, Iran), near the border of Iran-Iraq, causing hundreds of deaths, thousands of injuries, and building damage and collapse, mostly in Kermanshah. The epicenter was located in the Northwestern part of the Zagros mountain range, an active belt that originated from the Arabia-Eurasia collision and shook western regions of Iran. Before the occurrence of this earthquake in the Sarpol-e Zahab region, it was commonly thought that such a major event was unlikely where it occurred.

The region belongs to the Zagros mountain range, one of the youngest and most seismically active belts on Earth, originated by the Arabia-Eurasia collision in Late Paleogene, and extending from South-East Turkey to the south of Iran. The accommodation of the convergence between Arabia and Eurasia differs along the Zagros belt (Walpersdorf, et al., 2006). Tectonically, the principal differences in parts of Zagros are due to the orientations of major dextral faults and in their relationships with young thrusts and folds (Walker et al., 2003; Bachmanov et al., 2004).

Seismicity in Zagros is characterized mostly by moderate-size earthquakes ($M_w \leq 6$), with few sporadic events having a magnitude $M_w \geq 7$. Most of the earthquakes occur in the lower folded-sedimentary cover; in the southern part, in

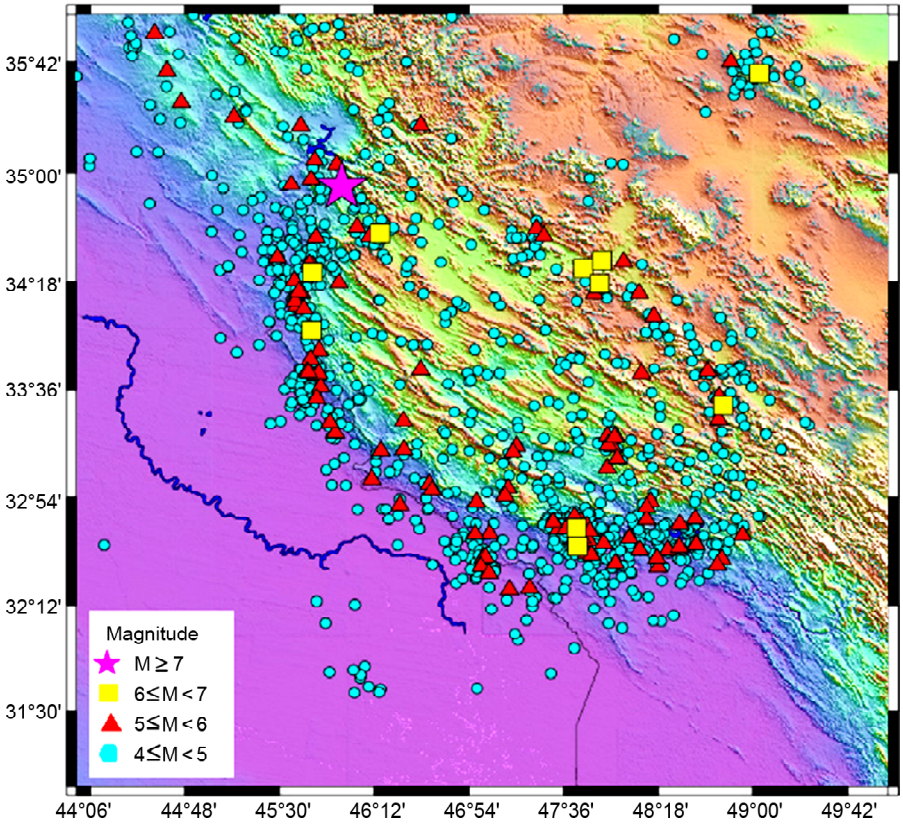

Figure 1. Seismicity of Sarpol-e Zahab and nearby regions with earthquakes M ≥ 4 that occurred between 1 December 1955 and 9 January 2020.

particular, the weak Hormuz salt at the base of the cover confines most faulting and limits the earthquake magnitudes up to 6.0 (Nissen et al., 2019). The northern part of Zagros, including the zone affected by the 2017 Sarpol-e Zahab earthquake with a magnitude of M_w 7.3, has experienced a smaller number of earthquakes than the southern part of it. In the northern part of Zagros, the crustal deformation occurs mostly seismically, while aseismic strain dominates crustal deformation in Southern Zagros (Ramezani et al., 2018; Palano et al., 2017; Mahood & Hamzehloo, 2008, 2011).

Earthquake nowcasting is a modern method of estimating seismic risk by evaluating the progress of the earthquake cycle in fault systems. Earthquake nowcasting evaluation is based on a new concept of time, termed 'natural time'. The nowcasting concept has studied (a new method of statistically classifying seismicity and seismic hazard), which examines the current uncertain situation of earthquake risk assessment in Sarpol-e Zahab and the surrounding areas, and then, time series analysis of interevent counts. Many of these earthquakes will be aftershocks of the last largest event. The rate of occurrence of small earthquakes has counted to nowcast the probability of occurrence of more significant earthquakes. The occurrence of various seismic events in the area allows studying the seismic cycle and earthquake potential score (EPS) within a 250-300 km radius of this region The nowcasting approach is used for major events of $M_w \geq 6$, often causing damage to infrastructure systems and adverse economic effects. Once the current state of the fault system in the defined area is better understood, it should be possible to better characterize the future state of the region and the calculation of forecast probabilities.

Kanamori (2003) illustrated that earthquake forecasting is the probabilistic assessment of general earthquake seismic hazards, including the frequency and magnitude of damaging earthquakes in a given area over years or decades. While forecasting is usually considered a type of prediction, earthquake forecasting is often differentiated from earthquake prediction, whose goal is to specify the time, location, and magnitude of future earthquakes with sufficient precision so that a warning can be issued.

2. Nowcasting Method

The nowcasting method is a concept borrowed from economics and finance (Rundle et al., 2016). It refers to the process of determining the uncertain state of the economy or markets at the current time by indirect means. Rundle et al. (2016) have applied this idea to seismically active regions, where the goal is to determine the current state of the fault system and its current level of progress through the earthquake cycle by counting the number of small earthquakes that occurred over time between two large earthquakes in a given region. As in financial nowcasting where the aim is to characterize the current dynamical state of the economy or in meteorological nowcasting where the goal is to describe the current uncertain state of weather conditions, the earthquake nowcasting in a seismogenic area seeks to define the current state of hazard, rather than to produce a forecast that looks ahead in time (Rundle et al., 2019, 2020). Recent studies have shown that nowcasting is a new technique for calculating the seismic risk level based on natural time (Rundle et al., 2019, 2020; Luginbuhl et al., 2018). This is emphasized that the earthquake cycle refers to repeated events in the seismic zone (Sornette & Knopoff, 1997). Nowcasting uses the catalog of seismicity in the region. Two earthquake magnitudes are selected, one large say M_λ, and one small say M_σ. The method utilizes the number of small earthquakes that occur between pairs of large earthquakes. A major advantage of nowcasting is that it relies on 'natural time', earthquake counts, between events rather than clock time, and the major advantage of using the natural time measure is that it eliminates the need for declustering a catalog to remove aftershocks from the background seismicity and results do not depend on the clock time dependence of the seismicity (Rundle et al., 2019, Panakkat, 2009). Small events can therefore be used as a kind of "clock" that marks the "natural time" between the large events. The count of small earthquakes since the last large earthquake is the natural time that has elapsed since the last large earthquake (Rundle et al., 2019; Panakkat & Adeli, 2009; Fox et al., 2022). Luginbuhl et al. (2018) by the recent 2004 M_w 9.0 Sumatra earthquake, the 2010 M_w 8.8 Maule, Chile earthquake,

and the 2011 M_w 9.1 Tohoku, Japan earthquake which make up half of the six largest earthquakes on record, analyzed the temporal clustering of large global earthquakes concerning natural time, or inter-event count, as opposed to regular clock time.

The Gutenberg-Richter magnitude-frequency relation can be used to show that the number of small earthquakes having magnitudes larger than M_σ but less than magnitude M_λ is an average known value *N*. *N* can be calculated by using the Gutenberg-Richter law for the average number *N* of earthquakes greater than *M*:

$$Log\, N = a - bM \tag{1}$$

where the *b* value is typically a number near 1, and the value of a is set by the level of seismicity in the region (Faghih et al., 2015). The *b* value is also set by the level of seismicity and might be lower or higher than 1, but based on Faghih et al. (2015) *b* value is considered 1.

The average number *N* of small earthquakes between large earthquakes will be called the mean inter-event count. Mathematically, we can express the progress through the regional earthquake cycle, or earthquake potential for a large earthquake to occur having a magnitude larger than M_λ, by computing the cumulative distribution function (CDF) of small earthquakes of magnitude larger than M_σ but less than $M_\lambda : M_\sigma \le M \le M_\lambda$.

To compute the CDF, we tabulate the number of small earthquakes for each large earthquake cycle from an appropriate database from global seismic catalogs including the United States Geological Survey (USGS) Catalog (U.S. Geological Survey 2017). We then use this to define the probability density function (PDF) and the CDF by standard methods (e.g., Bevington & Robinson, 2003). Once we have the CDF, we can then use the current count of small earthquakes $n(t)$ at time t to compute the current value of the CDF, $P\{n \le n(t)\}$. Note that t is the (calendar) time since the last large earthquake, and $n(t)$ is the number of small earthquakes since the last large earthquake. This value is defined to be the earthquake potential score (EPS) at time *t*:

$$EPS \equiv P\{n \le n(t)\} \tag{2}$$

The *EPS* is interpreted as the potential for the occurrence of the next large earthquake having a magnitude larger than M_λ within the defined geographic region. By construction, EPS will increase monotonically with time since the last large earthquake. It will reset to $EPS = P\{n \le n(t=0)\} = 0$ immediately after the next large earthquake, and then again begin to increase monotonically until the next large earthquake occurs. It is noted that the nowcasting method does not, a priori, involve a model; it is only a process of tabulating and interpreting data. However, to the extent that the results have meaning, it is a transparent way of estimating the progress of a region through the seismic cycle of large earthquakes. Since our analysis is independent of the rate of seismic, we can apply it either to the large geographic area used to obtain statistics or to any smaller region within the larger region. Rundle et al. (2016) emphasized that the nowcasting method yields no information about the future. For example, an EPS value of 50 in a location with few small earthquakes may reside in that state for many years. On the other hand, an EPS value of 50 in a very active location would see a rapid increase in EPS over a very short time.

3. Result and Discussion

It is noted that the presence of small earthquakes requires an estimation of the magnitude of completeness (M_c), which is the minimum magnitude of events that the network is likely to report without omission. The M_c parameter is not only defined by the network capability, but also is a crucial parameter for estimating the seismic rate and the b-value of the G-R distribution, at least for the most commonly used methods.

To assess M_c, the calculation of the a- and b-values of the G-R law as a function of the lowest magnitude was conducted using the maximum likelihood estimation to compute these parameters and their confidence limits. Using the maximum curvature method, the M_c and b-values are equal to 4.4 and 1.03 ± 0.06, respectively for the study region (Figure 2).

To evaluate the current state of earthquake hazards for the Sarpol-e Zahab area using the nowcasting method and natural time as the count of small earthquakes ($4.4 \le M_w \le 6$) since the last

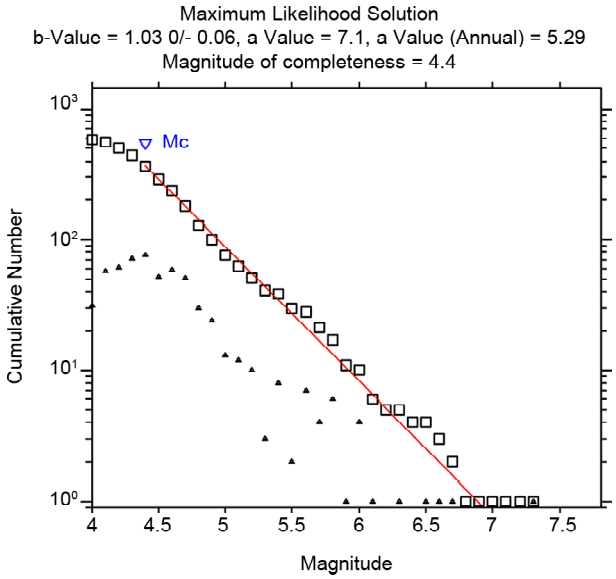

Figure 2. G-R plot of the cumulative number of events versus magnitude for Sarpol-e Zahab and adjacent regions. [Cumulative (squares) and non-cumulative (triangles) numbers are represented by squares, the red curve is the fitting curve].

large earthquake ($M_w \geq 6$), we initially consider $M_w \geq 4.4$ magnitude earthquakes within the range of radius 250 and 350 km around Sarpol-e Zahab. Since December 1, 1955, 643 earthquakes within a radius of 250 km and 1081 earthquakes within a radius of 350 km with $M_w \geq 4.4$ have occurred around Sarpol-e Zahab. It is noted that, among them, there were 7 and 11 earthquakes with $M_w \geq 6$ for the circle of radius 250 and 350 km, the most recent significant event of which occurred on 11 Nov 2017 with M_w 7.3.

Here, results are focused on defining the theoretical distribution of the interevent natural time. Time-dependent and time-independent fits have been considered in the data in the statistical seismology. The Time-independent exponential distribution is assumed to be an essential model, while time-dependent probability models, namely Weibull, gamma, and lognormal have been widely used in inter-event time modeling (Rundle et al., 2017; Nishenko & Bullard, 1987; Utsu, 1984; Yadav et al., 2010). Hence, six candidate probability distributions, namely normal, lognormal, gamma, exponential, Weibull, and inverse Gaussian are considered to characterize the observed natural time and are used to provide important modeling advantages of statistical seismology.

Based on the non-parametric Kolmogorov-Smirnov (K-S) test, Akaike information criterion (AIC), and Bayesian information criterion (BIC), Johnson et al. (1995), introduced model selection. To evaluate the current number of small earthquake counts, the cumulative distribution is the best-fit model in order to provide a numerical earthquake potential score for the studied area (Figures 3 and 4). The estimated value of the maximum likelihood model parameters are included in the Tables (1) and (2). The calculated K-S and AIC and BIC values related to the cumulative distribution function versus small interevent earthquakes for each conditions are shown in Figures (3) and (4).

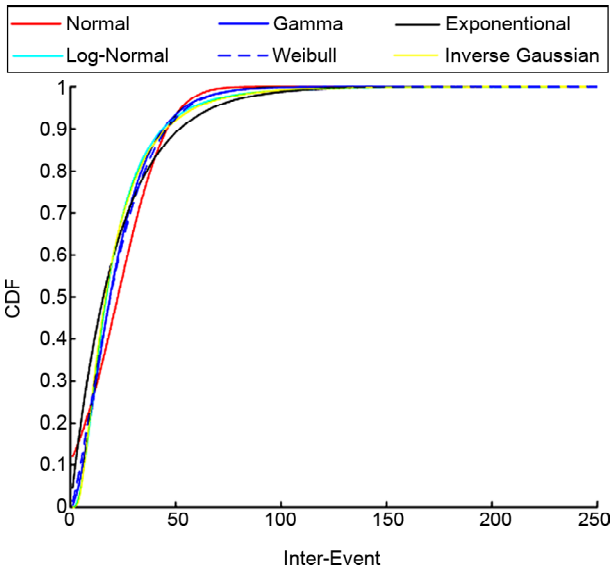

Figure 3. K-S statistical plots for interevent counts of small earthquakes between large earthquakes. CDF versus interevent earthquakes (M_σ=4.4, M_λ=5.5, R=250 km).

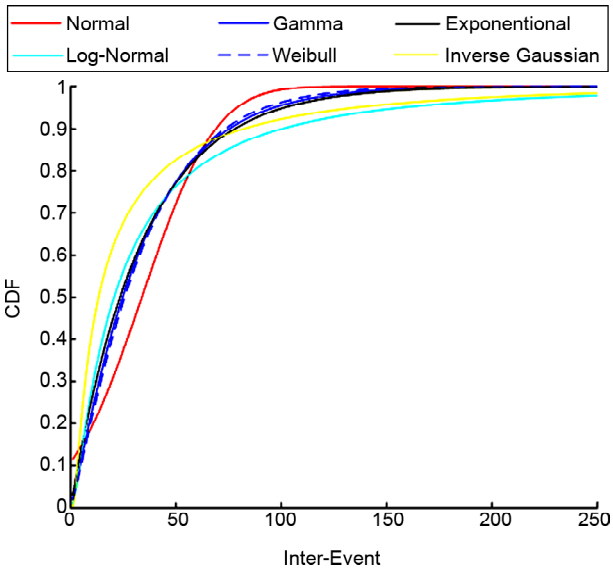

Figure 4. K-S statistical plots for interevent counts of small earthquakes between large earthquakes. CDF versus interevent earthquakes (M_σ=4.4, M_λ=5.5, R=350 km).

Table 1. Maximum likelihood model parameters ($M_\sigma = 4.4$, $M_\lambda = 5.5$, R=250 km).

Distribution	Model Section		
	K-S	AIC	BIC
Normal	0.246	1634.769	1636.385
Lognormal	0.258	2985.561	2987.177
Gamma	0.265	3389.838	3391.454
Weibull	0.242	3109.655	3111.271
Exponential	0.284	3027.967	3028.775
Inverse Gaussian	0.712	1313.814	1315.431

Table 2. Maximum likelihood model parameters ($M_\sigma = 4.4$, $M_\lambda = 5.5$, R=350 km).

Distribution	Model Section		
	K-S	AIC	BIC
Normal	0.165	85.213	84.224
Lognormal	0.174	125.549	124.559
Gamma	0.106	173.094	172.104
Weibull	0.089	168.021	167.032
Exponential	0.131	163.887	163.392
Inverse Gaussian	0.998	113.789	112.800

Table 3. Nowcast values for earthquakes in Sarpol-e Zahab region (on 9 Jan 2020).

Parameters			EPS (%)	Natural Time Count	Last Large Event		Best Fit Model	
M_σ	$M_\lambda \geq$	R(km)			Date	M	K-S	AIC-BIC
4	5.5	250	85	41	2019.01.06	5.6	Weibull	Normal
		350	71	45	2019.01.06	5.6	Weibull	Normal
4.4	5.5	250	86	41	2019.01.06	5.6	Weibull	Normal
		350	73	45	2019.01.06	5.6	Weibull	Normal
4	6	250	96	61	2018.11.25	6.3	Weibull	Normal
		350	49	65	2018.11.25	6.3	Gamma	Normal
4.4	6	250	97	60	2018.11.25	6.3	Weibull	Normal
		350	50	64	2018.11.25	6.3	Gamma	Normal

The studied distributions are ranked by the measurement of the AIC and K-S test statistical values, and the obtained data showed that the K-S test is the best-fit model, whereas according to the compromise between model complexity and model fit, AIC and BIC are the most suitable models (Johnson et al., 1995). The K-S test is recommended for comparing and validating the considered distributions based on two advantages, the non-parametric nature and the ability to evaluate the overall fitting analysis of the K-S plot.

The approximate K-S statistic values corresponding to the gamma and Weibull distributions appear to be the least among all K-S values. Thus, the K-S test indicates that the Weibull and gamma models are the most fitting to reflect the current earthquake catalog of Sarpol-e Zahab and its surrounding areas. Also, the AIC and BIC models for the normal distribution are the lowest of all competitive distributions (Table 3). Thus, although normal distribution is the most economical model, the gamma distribution is best suited to the natural time data observed (Figures 3 and 4 and Tables 1 and 2).

Figure (5) shows the results of the EPS value calculations for $M_\lambda \geq 5.5$ and 6.0 within a 350 km radius of the Sarpol-e Zahab area. The CDFs $P[n \leq n(t)]$ of the histogram values are shown by the blue curves. Bold circles represent the number of small earthquakes since the last large earthquake. The blue data-derived curve is the best-fitting Weibull distribution. The obtained EPS score for $M_w \geq 5.5$ recovered to an average value of 73%, showing that this area is in a comparatively mature seismic state, while the current EPS for $M_w \geq 6.0$ is estimated at 50%, suggesting that the studied region is halfway through its great earthquake cycle (Table 3 and Figure 5).

We used the natural time concept and the nowcasting approach to evaluate large earthquakes that occurred during the time period and in the study area to provide a seismic map of the considered geographical region. Figure (6) depicts the estimated current EPS values as a risk map (Wessel & Smith, 1995, Mirhoseini et al., 2021). The hazard level is lower in regions of lower altitudes and higher in areas of elevated altitudes. The elevated altitudes describe active and unstable regions with high risk (Faghih, 2015).

The increasing blue curve is the $CDF = P[n \leq n(t)]$ calculated from the large earthquake intervals. 64 earthquakes have occurred in the

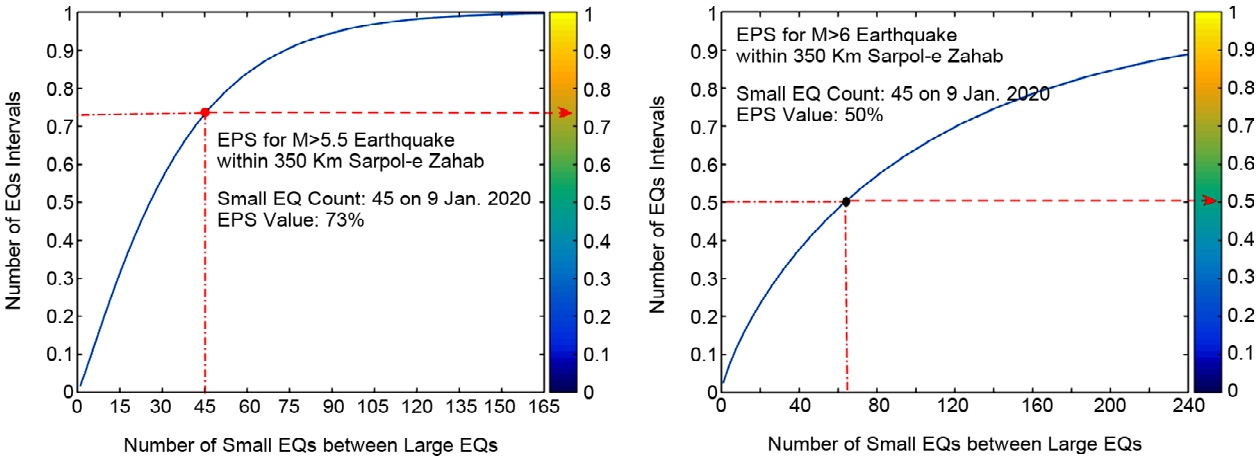

Figure 5. Nowcast for the $M_w \geq 5.5$ and 6.0 earthquakes in the Sarpol-e Zahab region (R = 350 km). Blue curves are the best CDF. The Bold dots represent the current number of small earthquakes after the last large earthquake of M_w 5.5 and 6.0 on 6 January 2019 and 25 November 2018, respectively.

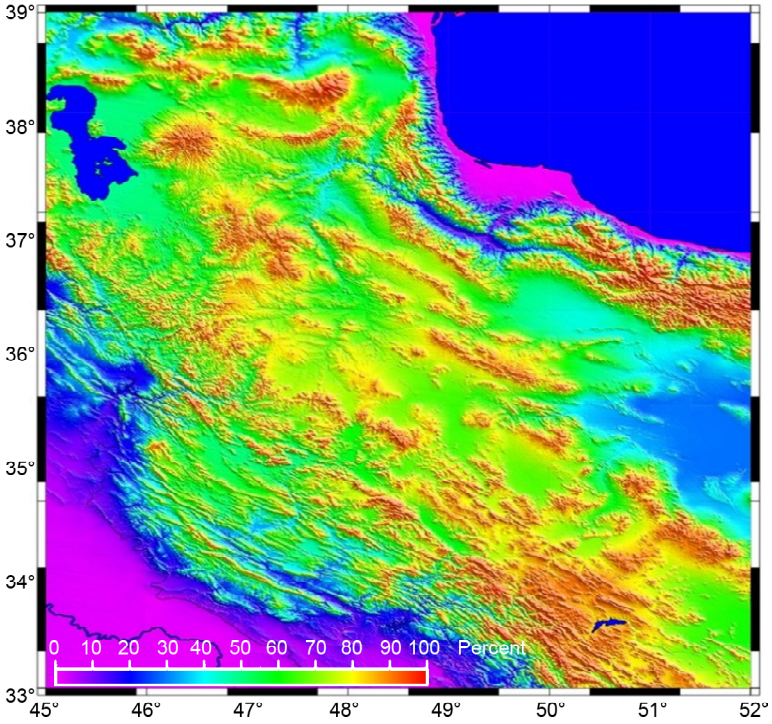

Figure 6. Current state of earthquake hazard for Kermanshah region.

area with $M_w \geq 4.4$, since the last $M_w \geq 6.0$ on 25 November 2018, while for the last $M_w \geq 5.5$ on 6 January 2019, we had only 45 earthquakes. After the last large earthquake, the natural time count of $M_w \geq 6.0$ events using the cumulative number of small earthquakes N and the estimated current potential magnitude M_P of the forthcoming great earthquake at the present time is given by:

$$M_P = M_C + \left(\frac{1}{b}\right)\log N_S \qquad (3)$$

where M_c reflects the catalogue completeness magnitude, Ns is the current count of small earthquakes increasing in time, and b denotes the G-R b-value. By applying Equation 3 with $M_c = 4.4$, $b = 1.19$, and $N_s = 64$ in the Sarpol-e Zahab region, an approximation of the possible magnitude of the latest potential great earthquake as $M_P = 5.9$ can be found (Figure 7). This is consistent with the potential for the next earthquake in Figure (2) (G-R magnitude frequency data of the Sarpol-e Zahab), which suggests that an earthquake with a magnitude of nearly 5.9 will occur in the near future.

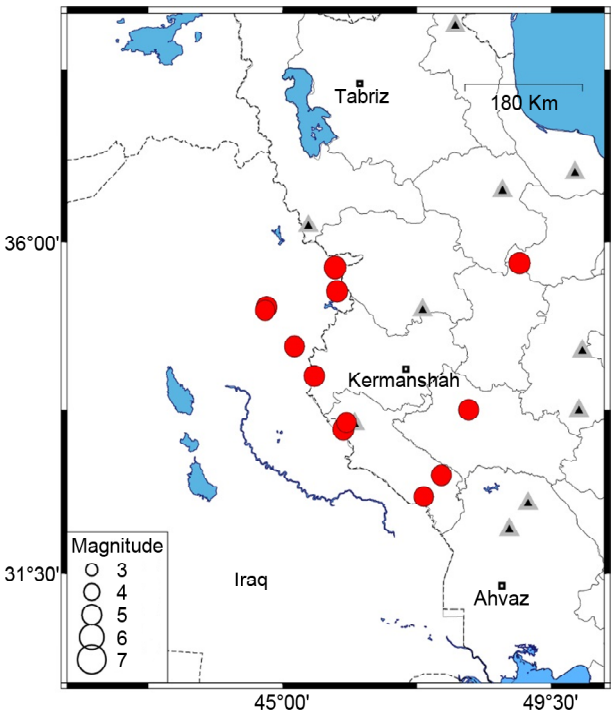

Figure 7. Seismicity of study region from January 2020 to February 2024, $M_w > 5$.

Figure (7) shows the Seismicity of the study region from January 2020 to February 2024, $M_w > 5$. This figure shows 12 earthquakes with $M_w > 5$ have occurred within a 350 km radius of Sarpol-e Zahab.

The BASS (branching aftershock sequence) model proposed by Holliday et al. (2008) is a preferred alternative to the widely studied epidemic-type aftershock sequence model. In the BASS model an initial, or seed, earthquake is specified. The subsequent earthquakes are obtained from the statistical distributions of magnitude, time, and location. The magnitude scaling is based on a combination of the Gutenberg-Richter scaling relation and the modified Bath's law for the scaling relation of aftershocks relative to the magnitude of the seed earthquake. Omori's law specifies the distribution of earthquake times, and a modified form of Omori's law specifies the distribution of earthquake locations. Since the BASS model is specified by the four scaling relations, it is fully self-similar.

In the BASS model, the distribution of aftershocks is checked after a mainshock, but in the nowcasting, the seismicity of a region with all the big and small earthquakes that have occurred is used to process of determining the uncertain state of the seismicity at present where the goal is to estimate the current state of risk, the current state of the fault system, and its current level of progress through the earthquake cycle.

According to the cycles of earthquakes in each region, measures can be taken for earthquake preparedness and mitigation, to reduce the risk before an earthquake occurs. More studies in smaller areas, micro zonation of earthquake risk can be estimated, and effective measures can be taken. Strengthening structures, and checking the condition of infrastructure systems, vital and relief arteries is one of the first measures.

4. Conclusions

The goal of nowcasting is to determine the current state of the fault system, or put another way, the current state of progress through the earthquake cycle. This is in contrast to forecasting, which is the calculation of probabilities of future large earthquakes. We applied the nowcasting idea to the practical development of methods to estimate the current risk state for the Sarpol-e Zahab in Kermanshah region.

In the nowcasting method, we construct the cumulative probability distribution function (CDF) for the number of small earthquakes between large earthquakes during a sequence of earthquake cycles. These cycles occur in a large region around the area of interest, typically a local region around a specific geographic location. An advantage of this method is that it offers a systematic means of ranking locations as to their current exposure to earthquake hazards. We calculate an Earthquake Potential Score (EPS) that is found by determining the number of small earthquakes since the last large earthquake, by using the CDF found from the regional earthquake cycles.

For dates between 1st December 1955 and 9 January 2020, we used the nowcasting approach to estimate earthquake hazard in Kermanshah province, namely Sarpol-e Zahab and the surrounding area. The nowcasting applicability requires that the studied seismicity satisfies the G-R frequency magnitude with a reasonable approximation. The least-squares fit of the truncated G-R gives $M_{\max} \approx 7.0$.

In the nowcasting approach, we calculate the CDF for the number of small earthquakes between

large earthquakes during a sequence of earthquake cycles. The Weibull distribution has the best goodness-fit tests within a radius of 250 and 350 km around the studied region. Choosing the search radius depends on data distributed in the study region. With different radii similar to 200 km, we didn't find any reliable relation in the earthquake cycle. The EPS was calculated as the cumulative number of small earthquakes since the last large event. A statistical measurement of observed seismicity is crucial for understanding earthquake dynamics and future risk. The EPS values for $M \geq 6.0$ occurrences, within radius circles of 350 km neighboring Sarpol-e Zahab city are 50%, suggesting that the studied region is halfway through its great earthquake cycle. Active regions with EPS estimated at more than 90% for $M_w \geq 6.0$ are near the end of their current earthquake cycle for events $M_w \geq 6.0$.

This method offers a rapid and easily reproducible model to estimate the current level of progress through the earthquake cycle for any local region subject to seismic hazard worldwide.

Acknowledgments

The author thanks the international institute of earthquake engineering and seismology (IIEES) for its support. The author thanks the referees who increased the scientific weight of the manuscript with their careful review and valuable comments, too.

References

Bachmanov, D.M., Trifonov, V.G., Hessami, K.T., Kozhurin, A.I., Ivanova, T.P., Rogozhin, E.A., Hademi, M.C., & Jamali, F.H. (2004). Active faults in the Zagros and central Iran. *Tectonophysics*, *380*(3-4), 221-241.

Berberian, M. (1976). Contribution to the seismotectonics of Iran (Part II). *Geol. Surv. Iran*, Report No. 39, 516p.

Bevington P.R., & Robinson D.K. (2003). *Data Reduction and Error Analysis in the Physical Sciences*. Boston, McGraw-Hill.

Faghih, A., Esmaeilzadeh Soudejani, A., Nourbakhsh, A. & S. Rokni. (2015). Tectonic geomorphology of high Zagros ranges, SW Iran: an initiative towards seismic hazard assessment. *Environ. Earth Sci.*, *74*, 3007-3017.

Fox, G. C., Rundle, J. B., Donnellan, A., & Feng, B. (2022). Earthquake nowcasting with deep learning. *GeoHazards*, *3*(2), 199-226. https://doi.org/10.3390/geohazards3020011.

Gentili, S., Peresan, A., Talebi, M., Zare, M., & Di Giovambattista, R. (2019). A seismic quiescence before the 2017 Mw 7.3 Sarpol-e Zahab (Iran) earthquake: Detection and analysis by improved RTL method. *Physics of the Earth and Planetary Interiors*, *290*, 10-19. https://doi.org/10.1016/j.pepi.2019.02.010.

Holliday, J.R., Turcotte, D.L., & Rundle, J.B. (2008). Self-similar branching of aftershock sequences. *Physica. A*, *387*(4), 933-943. https://doi.org/10.1016/j.physa.2007.09.045.

Johnson, N.L., Kotz, S., and Balakrishnan, N. (1995). *Continuous Univariate Distributions*. Wiley.

Kanamori, H. (2003). 72 Earthquake prediction: An overview. *In International Geophysics/International Geophysics Series*, 1205-1216. https://doi.org/10.1016/s0074-6142(03)80186-9.

Luginbuhl, M., Rundle, J.B., & Turcotte, D.L. (2018). Natural time and nowcasting earthquakes: Are large global earthquakes temporally clustered? *Pure and Applied Geophysics*, *175*(2), 661-670. https://doi.org/10.1007/s00024-018-1778-0.

Mahood, M., & Hamzehloo, H. (2008). Estimation of coda wave attenuation in East Central Iran. *Journal of Seismology*, *13*(1), 125-139. https://doi.org/10.1007/s10950-008-9130-2.

Mahood, M., & Hamzehloo, H. (2011). Variation of intrinsic and scattering attenuation of seismic waves with depth in the Bam region, East-Central Iran. *Soil Dynamics and Earthquake Engineering*, *31*(10),1338-1346. https://doi.org/10.1016/j.soildyn.2011.05.010.

Mirhoseini, S. F., Mahood, M., Tahernia, N., Dorostian, A., & Akasheh, B. (2021). Case study of earthquake probability using natural time and nowcasting of the Sarpol-e Zahab region in Kermanshah, Iran. *Pure and Applied Geophysics*,

178(4), 1181-1191. https://doi.org/10.1007/s00024-021-02699-x.

Nishenko, S.P., & Buland, R. (1987). A generic recurrence interval distribution for earthquake forecasting. *The Bulletin of the Seismological Society of America*, *77*(4), 1382-1399. https://doi.org/10.1785/bssa0770041382

Nissen, E.A., Ghods. A., Ezgi Karasozen. E., & Elliot. J.R. (2019). The 12 November 2017 Mw 7.3 Ezgeleh-Sarpolzahab (Iran) earthquake and active tectonics of the Lurestan arc. *J. Geophys. Res.*, *124*, 1-19.

Palano, M., Imprescia, P., Agnon, A., & Gresta, S. (2018). An improved evaluation of the seismic/geodetic deformation-rate ratio for the Zagros Fold-and-Thrust collisional belt. *Geophysical Journal International*, *213*(1), 194-209. https://doi.org/10.1093/gji/ggx524.

Panakkat, A., & Adeli, H. (2009). Recurrent neural network for approximate earthquake time and location prediction using multiple seismicity indicators. *Computer-Aided Civil and Infrastructure Engineering*, *24*(4), 280-292. https://doi.org/10.1111/j.1467-8667.2009.00595.x.

Ramezani, A., Abbaspour, R.A., & Mojarab, M. (2018). Assessment of the M8 algorithm by spatial integrating of alarms (case study: Sarpol-e Zahab earthquake). *Journal of Environmental Hazard Management*, *4*.

Rundle, J.B., Giguere, A., Turcotte, D.L., Crutchfield, J.P., & Donnellan, A. (2019). Global seismic nowcasting with Shannon information entropy. *Earth and Space Science*, *6*(1), 191-197. https://doi.org/10.1029/2018ea000464

Rundle, J.B., Luginbuhl, M., Giguere, A., & Turcotte, D.L. (2017). Natural time, nowcasting and the physics of earthquakes: estimation of seismic risk to global megacities. *Pure and Applied Geophysics*, *175*(2), 647-660. https://doi.org/10.1007/s00024-017-1720-x.

Rundle, J.B., Luginbuhl, M., Khapikova, P., Turcotte, D.L., Donnellan, A., & McKim, G. (2020). Nowcasting great global earthquake and tsunami sources. *Pure and Applied Geophysics*, *177*(1), 359-368. https://doi.org/10.1007/s00024-018-2039-y.

Rundle, J.B., Turcotte, D.L., Donnellan, A., Ludwig, L.G., Luginbuhl, M., & Gong, G. (2016). Nowcasting earthquakes. *Earth and Space Science*, *3*(11), 480-486. https://doi.org/10.1002/2016ea000185.

Sornette, D., & Knopoff, L. (1997). The paradox of the expected time until the next earthquake. *The Bulletin of the Seismological Society of America*, *87*(4), 789-798. https://doi.org/10.1785/bssa0870040789.

USGS (2017). http://earthquake.usgs.gov/earthquakes, Accessed in 2017.

Utsu, T. (1984). Estimation of parameters for recurrence models of earthquakes. *Bulletin of Earthquake Research Institute*, *59*, 53-66, University of Tokyo.

Walker, R., Jackson, J., and Baker, C. (2003). Surface expression of thrust faulting in eastern Iran: source parameters and surface deformation of the 1978 Tabas and 1968 Ferdows earthquake sequences., *Geophys. J. Int.*, *152*, 749-765.

Walpersdorf, A., Hatzfeld, D., Nankali, H., Tavakoli, F., Nilforoushan, F., Tatar, M., Vernant, P., Chéry, J., & Masson, F. (2006). Difference in the GPS deformation pattern of North and Central Zagros (Iran). *Geophysical Journal International*, *167*(3), 1077-1088. https://doi.org/10.1111/j.1365-246x.2006.03147.x.

Wessel, P., & Smith, W. H. F. (1995). New version of the generic mapping tools. *Eos*, *76*(33), 329. https://doi.org/10.1029/95eo00198.

Yadav, R.B.S., Tripathi, J.N., Rastogi, B.K., Das, M.C., & Chopra, S. (2010). Probabilistic assessment of earthquake recurrence in northeast India and adjoining regions. *Pure and Applied Geophysics*, *167*(11), 1331-1342. https://doi.org/10.1007/s00024-010-0105-1.